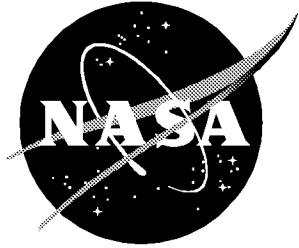


NASA/TM-2000-210283



Three Averaging Techniques for Reduction of Antenna Temperature Variance Measured by a Dicke Mode, C-Band Radiometer

*Anne I. Mackenzie and Roland W. Lawrence
Langley Research Center, Hampton, Virginia*

May 2000

The NASA STI Program Office . . . in Profile

Since its founding, NASA has been dedicated to the advancement of aeronautics and space science. The NASA Scientific and Technical Information (STI) Program Office plays a key part in helping NASA maintain this important role.

The NASA STI Program Office is operated by Langley Research Center, the lead center for NASA's scientific and technical information. The NASA STI Program Office provides access to the NASA STI Database, the largest collection of aeronautical and space science STI in the world. The Program Office is also NASA's institutional mechanism for disseminating the results of its research and development activities. These results are published by NASA in the NASA STI Report Series, which includes the following report types:

- **TECHNICAL PUBLICATION.** Reports of completed research or a major significant phase of research that present the results of NASA programs and include extensive data or theoretical analysis. Includes compilations of significant scientific and technical data and information deemed to be of continuing reference value. NASA counterpart of peer-reviewed formal professional papers, but having less stringent limitations on manuscript length and extent of graphic presentations.
- **TECHNICAL MEMORANDUM.** Scientific and technical findings that are preliminary or of specialized interest, e.g., quick release reports, working papers, and bibliographies that contain minimal annotation. Does not contain extensive analysis.
- **CONTRACTOR REPORT.** Scientific and technical findings by NASA-sponsored contractors and grantees.

- **CONFERENCE PUBLICATION.** Collected papers from scientific and technical conferences, symposia, seminars, or other meetings sponsored or co-sponsored by NASA.
- **SPECIAL PUBLICATION.** Scientific, technical, or historical information from NASA programs, projects, and missions, often concerned with subjects having substantial public interest.
- **TECHNICAL TRANSLATION.** English-language translations of foreign scientific and technical material pertinent to NASA's mission.

Specialized services that complement the STI Program Office's diverse offerings include creating custom thesauri, building customized databases, organizing and publishing research results . . . even providing videos.

For more information about the NASA STI Program Office, see the following:

- Access the NASA STI Program Home Page at <http://www.sti.nasa.gov>
- Email your question via the Internet to help@sti.nasa.gov
- Fax your question to the NASA STI Help Desk at (301) 621-0134
- Telephone the NASA STI Help Desk at (301) 621-0390
- Write to:
NASA STI Help Desk
NASA Center for AeroSpace Information
7121 Standard Drive
Hanover, MD 21076-1320

NASA/TM-2000-210283



Three Averaging Techniques for Reduction of Antenna Temperature Variance Measured by a Dicke Mode, C-Band Radiometer

*Anne I. Mackenzie and Roland W. Lawrence
Langley Research Center, Hampton, Virginia*

National Aeronautics and
Space Administration

Langley Research Center
Hampton, Virginia 23681-2199

May 2000

Acknowledgments

This work was performed by a team of five engineers belonging to the Radiometer Group of the Sensors Research Branch at NASA Langley Research Center. These people were Roland W. Lawrence, Anne I. Mackenzie, William L. Munden, Terry L. Mack, and Michael J. Scherner. Roland Lawrence provided technical direction, inspiration, and assistance with the RF design and troubleshooting. William Munden assisted with the RF and electronic system design and grounding improvements and provided the SCR power amplifier for the temperature control system heater strips. Terry Mack assembled the PC, installed the software, provided counseling on the use of Labview, designed the temperature control system, and fabricated and assembled a large portion of the radiometer. Michael Scherner purchased the components, provided lab equipment and instruction, and assisted greatly with calibrations.

The work was funded by the Airborne C-Band Microwave Radiometer Program led by the NASA Goddard Research Center. The Program Manager was Larry Hilliard; the Principal Investigator was Edward Kim.

The use of trademarks or names of manufacturers in this report is for accurate reporting and does not constitute an official endorsement, either expressed or implied, of such products or manufacturers by the National Aeronautics and Space Administration.

Available from:

NASA Center for AeroSpace Information (CASI)
7121 Standard Drive
Hanover, MD 21076-1320
(301) 621-0390

National Technical Information Service (NTIS)
5285 Port Royal Road
Springfield, VA 22161-2171
(703) 605-6000

Contents

Abstract	1
Introduction	1
Background	1
Experiment Overview	4
Acronyms and Abbreviations	6
Radiometer Design	7
Radio Frequency Signal Path	7
Video Signal Path	8
Temperature Control System	9
Labview Controls and Digital Recording	9
Radiometer Characterization: Calibration of System Gain, Noise Diode Temperature, and System Noise Temperature	10
Comparison of the Effects of Averaging Techniques on Antenna Temperature Variances	13
Calculations Common to the Three Averaging Methods	13
Antenna Data Averaging with Variable Duty Cycle	14
Reference Data Averaging	14
System Gain Averaging	15
Results	15
Calculation of Improvement for Different Antenna Duty Cycles	17
Actual Versus Theoretical Reduction in ΔT by Using Asymmetric Chop and Reference Averaging	19
Conclusions	20
Future Work: Stability Analysis of Calculated $T_{REF+SYS}$ and System Gain Using Allan Variances	21
Appendix A - RF Component List	23
Appendix B - Electronic Board Schematics	23
Appendix C - Temperature Control System Schematic	26
Appendix D - Allan Variance	27
References	27
Related Reading	28

Abstract

As new radiometer technologies provide the possibility of greatly improved spatial resolution, their performance must also be evaluated in terms of expected sensitivity and absolute accuracy. As aperture size increases, the sensitivity of a Dicke mode radiometer can be maintained or improved by application of any or all of three digital averaging techniques: antenna data averaging with a greater than 50% antenna duty cycle, reference data averaging, and gain averaging. An experimental, noise-injection, benchtop radiometer at C-band showed a 68.5% reduction in ΔT after all three averaging methods had been applied simultaneously. For any one antenna integration time, the optimum 34.8% reduction in ΔT was realized by using an 83.3% antenna/reference duty cycle.

Introduction

Background

Since the first use of passive microwave measurements to observe the Earth from space aboard the Russian satellite Cosmos 243 in 1968, microwave radiometry has developed into a useful tool in the science of remote sensing. Over the past three decades, the science of interpreting microwave radiometric data has also developed, and although some minor disagreements may exist, generally the sensitivities, absolute accuracies, and frequencies required for radiometric measurements of various geophysical parameters are known. The usefulness of microwave remote sensing data can generally be characterized in terms of sensitivity, accuracy, and spatial resolution.

The configuration of the four-frequency Special Sensor Microwave/Imager (SSM/I) has been extremely successful, yielding substantial measurement accuracy. The spatial resolution ranged from 15 by 13 km at 85.5 GHz to 69 by 43 km at 19.35 GHz [1]; the accuracy was within 1.2 K for a scene temperature of 300 K. The SSM/I achieved this accuracy by using a calibration concept which included a rotating reflector and feed assembly spinning about a central axis (see figure 1), providing a view of a stationary warm load and a view of cold space during each scan. The result was an end-to-end calibration per revolution, approximately once each 1.9 s (31.6 rpm rotation). This calibration approach was simple and effective for use with the 24 by 26 in. SSM/I primary antenna.

The desire for passive microwave measurements of improved spatial resolution and the development of radiometer and antenna technologies have resulted in several studies to investigate large aperture radiometer systems [2]. These systems may use aperture synthesis, phased arrays, or reflectors. For example, the Ocean salinity Soil moisture Integrated Radiometric Imaging System (OSIRIS) concept uses a 6- to 8-m rotating mesh reflector, pictured in figure 2. Such a concept will not easily accommodate the "SSM/I like" calibration approach because of the mechanical difficulties associated with the aperture's size. The radiometer will likely rely on internal calibration and improved instrument stability. Pushbroom concepts that provide improved spatial resolution result in similar calibration challenges.

While these new technologies provide the possibility of greatly improved spatial resolution, their performance must also be evaluated in terms of expected sensitivity and absolute accuracy. The effort discussed here is intended to be applied to an ultra-stable radiometer concept that will include internal calibration techniques and may provide improved sensitivity. Such a radiometer may enable the large aperture systems required to provide the desired spatial resolution.

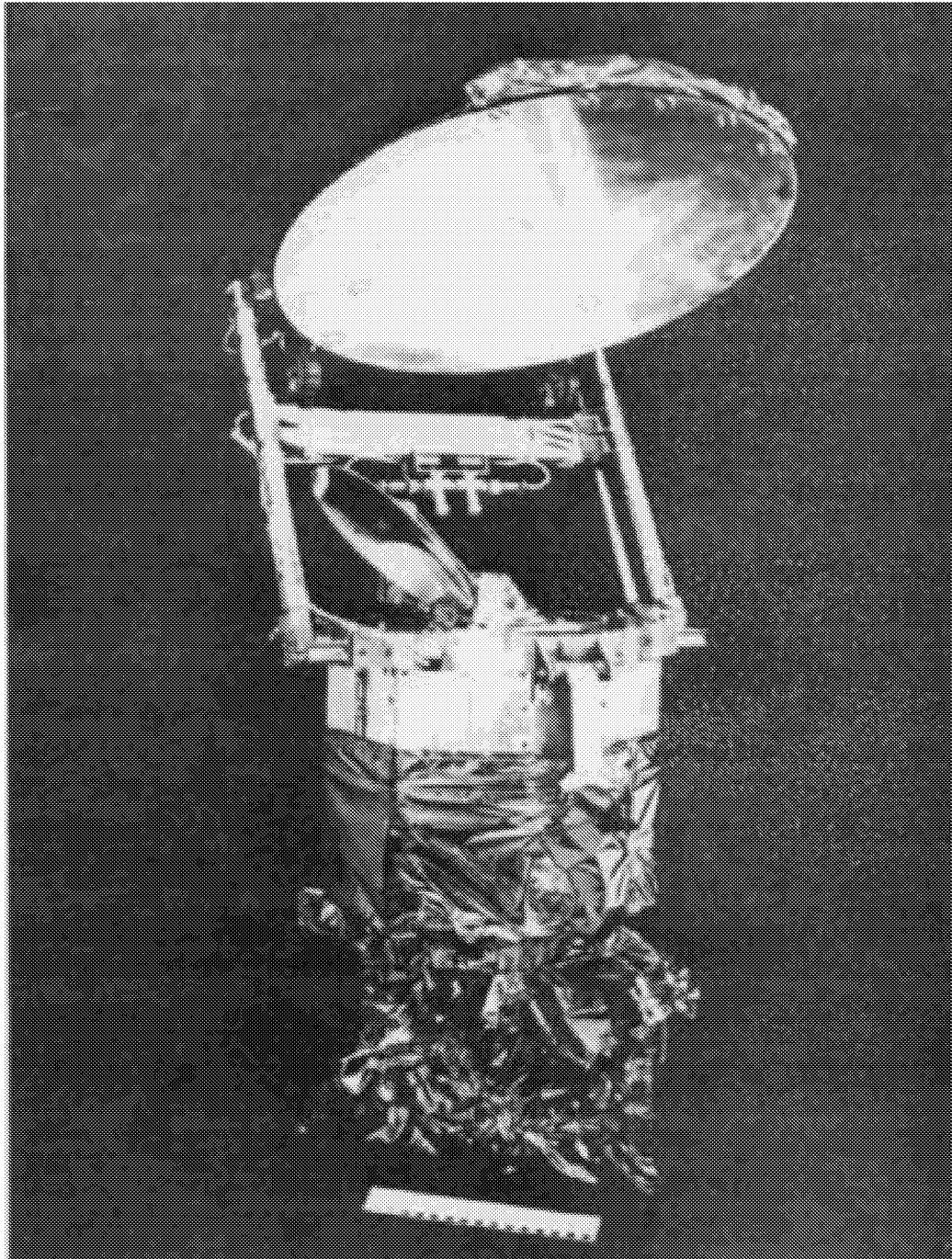


Figure 1. Photograph of an SSM/I radiometer prototype [1].

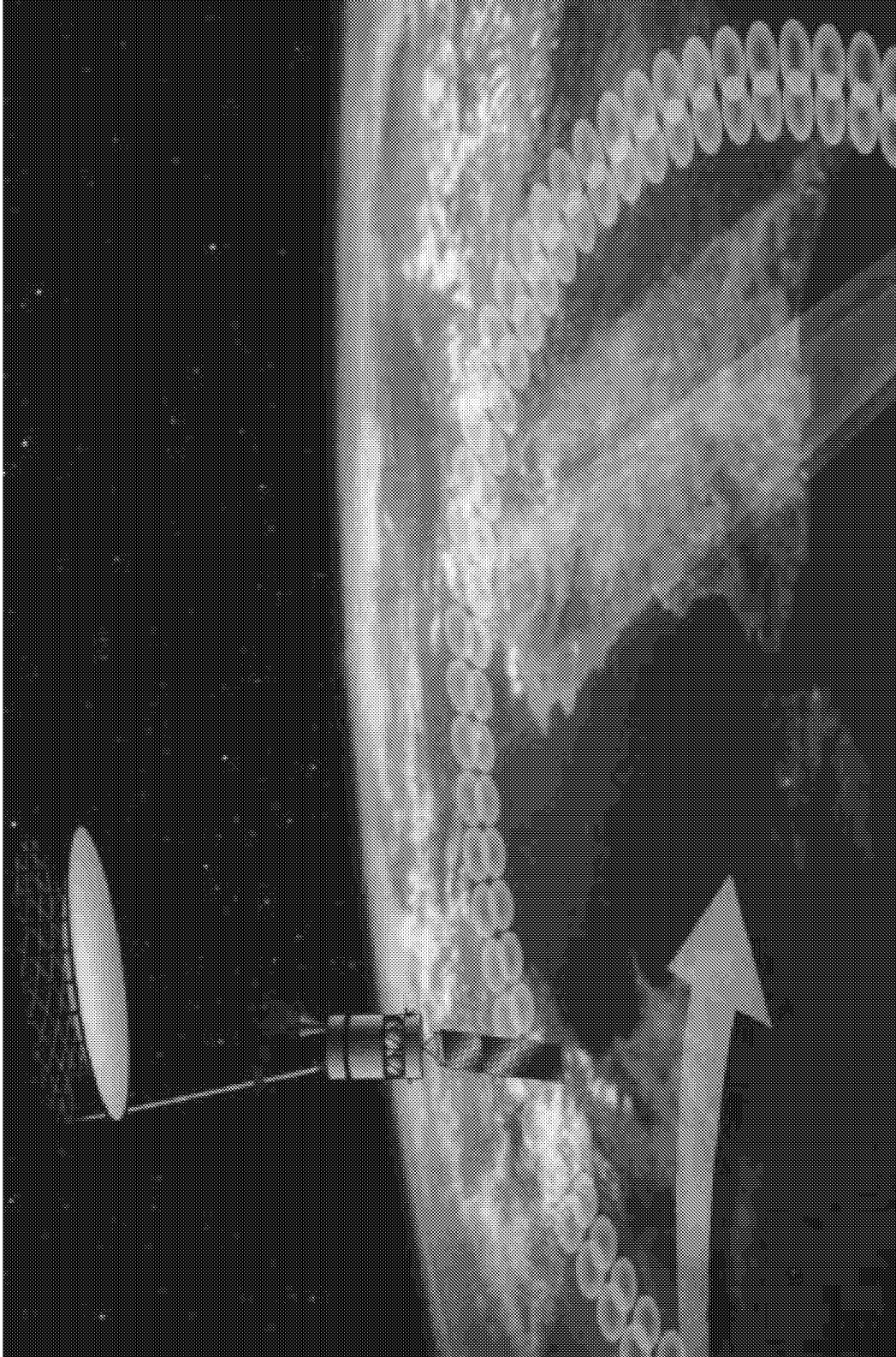


Figure 2. Artist's concept of the OSIRIS radiometer.

Experiment Overview

Sensitivity, or ΔT , is limited by the time available for antenna looks. One way to maintain radiometric accuracy and sensitivity, while increasing spatial resolution, is to spend a greater proportion of the available time looking at the scene rather than the reference. In fact, the sensitivity of a Dicke mode radiometer [3] can be improved significantly by application of any or all of three digital averaging techniques: antenna data averaging with a greater than 50% antenna duty cycle, reference data averaging, and gain averaging. The amount of each type of averaging that is beneficial depends upon the reference and gain stabilities of the particular radiometer in use.

Reference averaging is possible because the reference is stable for some time longer than the time required to view the scene for each antenna calculation. In a nonideal instrument, the amount of reference averaging is limited by the stability of the temperature reference and the system noise temperature. Changes in these quantities limit one's ability to remove offset variations and can add error to the estimate of T_{ANT} if the averaging is carried too far. Similarly, the gain is expected to be stable for some time longer than the scene time. Consequently, another way to reduce white noise in the antenna measurements is to average the gain over some time dependent on the stability of the noise source, RF detector, and amplifiers.

To demonstrate these averaging techniques, a 6.8 GHz (C-band), Dicke mode, noise-injection radiometer was built and tested in the Radiometer Laboratory of the Sensors Research Branch at NASA Langley Research Center. Hardware improvements to reduce the 1/f electronic noise, to reduce the physical temperature changes within the radiometer, or to reduce the effects of physical temperature changes might have been beneficial to the test radiometer but were not explored in the experiment.

Bremer's 1979 paper, *Improvement of Scanning Radiometer Performance by Digital Reference Averaging* [4], recommended the use of digital reference averaging, with an asymmetric scene/reference chop mode. A formula was developed to predict the improvement so gained, dependent on the fraction of each pixel's scan time during which scene information was collected and the number of reference points averaged. For an ideal Dicke mode radiometer with no linear temperature drift, it was demonstrated that

$$\Delta T_{NP} \propto k \quad (1)$$

$$k = \sqrt{\frac{1}{q} + \frac{1}{N(1-q)}} \quad (2)$$

where ΔT_{NP} = the ΔT due to white noise, q = antenna (scene) duty cycle, and N = number of reference points averaged. For a symmetric chop mode with no reference averaging, $q = 0.5$ and $N = 1$, making $k = 2$. As q increases to 1 and N becomes arbitrarily large, the "k factor" approaches 1. Thus, it is theoretically possible to reduce ΔT_{NP} by 1/2, using both reference averaging and an asymmetric chop mode. In the results discussion, the actual improvement of the experimental radiometer is compared against the theoretical improvement as predicted by (2).

For the test radiometer, a maximum of 68.5% improvement in ΔT , that is, a 68.5% reduction in the estimated antenna temperature standard deviation, was obtained by using the three averaging methods simultaneously. Relative to the improvement obtained by simply collecting

data at a 50% antenna duty cycle and averaging antenna temperatures, the maximum additional reduction in standard deviation was 34.8%. This optimum result was obtained at an 83.3% antenna duty cycle, with reference averaging for 22.7 s and gain averaging for 199.9 s.

The antenna data averaging method required that the antenna/reference switching pattern be altered from the usual 50% duty cycle to provide proportionally more antenna data points than reference data points. Consecutive antenna data were then averaged together before calculating antenna temperatures. Reference data needed for each temperature calculation were taken from intervals before and after the times when the antenna data were collected, so that equal numbers of points for antenna and reference data could be used per temperature calculation. For the reference averaging method, reference data were integrated over more points than the antenna data. The use of variable duty cycles, as implemented in the experiment, provided less frequent antenna temperatures than were obtained by using a 50% duty cycle without averaging. However, the use of variable duty cycles provided the same frequency of antenna temperatures, with a smaller variance than were obtained by using a 50% duty cycle and averaging.

Data were collected at each of five antenna duty cycles from 50% to 91.6%, with higher duty cycles allowing the averaging of more antenna data points for each antenna temperature calculation. Antenna temperatures were then calculated for 1-hr periods by using antenna averaging alone; then antenna and reference averaging together; and finally, antenna, reference, and gain averaging together. The variances of the resulting antenna temperatures by each technique were compared against the variance for the 50% duty cycle with no reference or gain averaging.

The following sections describe the radiometer design, radiometer characterization, calculation methods, and the comparison of measurements made by using the various averaging techniques. The compiled results for all data sets are presented in tables and graphs showing the consecutive improvements by each averaging method. The appendices contain details of the RF components, the electronic board schematics, the temperature control system schematic, and a discussion of the Allan variance method.

Acronyms and Abbreviations

A/D	Analog to digital converter
ANT	Antenna
B	Predetection bandwidth
DAQ	Data acquisition
dc	Direct current
<i>DIFF</i>	Difference
<i>DIODE</i>	Noise diode
ENR	Excess noise ratio
f	Frequency
G_{SYS}	Radiometer system gain
<i>INIT</i>	Initial, at the beginning of data recording
k	Factor proportional to the white noise content in ΔT
LNA	Low noise amplifier
M	Number of samples in a subgroup
N	Total number of samples for which the Allan variance is to be determined
<i>NP</i>	White noise power
PC	Personal computer
q	Antenna duty cycle expressed as a fraction
REF	Reference, a termination whose physical temperature is constant
RF	Radio frequency
RTD	Resistive thermal device
TEC	Thermoelectric cooler
SW	Switch
<i>SYS</i>	Radiometer system
T	Noise temperature
T_{COLD}	Noise temperature of the cryogenic termination
T_{DIFF}	Noise temperature difference, $T_{ANT+SYS} - T_{REF+SYS}$
T_{HOT}	Noise temperature of the thermal termination
TTL	Transistor-transistor logic
V_{COLD}	Measured voltage at the radiometer output when a cryogenic termination is connected to the radiometer input
V_{HOT}	Measured voltage at the radiometer output when a thermal termination is connected to the radiometer input
x	One sample of a random process
Δt	Time interval between samples
ΔT	Noise temperature standard deviation, or sensitivity
ΔT_{NP}	Noise temperature standard deviation due to white noise
τ	Integration period for an Allan Variance calculation
τ_s	Dicke switching period

Radiometer Design

Figure 3 depicts the major components of the experimental, bench-top radiometer, which was a test bed for the Airborne C-Band Microwave Radiometer flown by NASA Goddard. The Labview control program, RF and video sections, and temperature control system were custom built at Langley Research Center. Purchased components included a Pentium processor PC, Labview software, a National Instruments data acquisition board, Lightwave and Omega temperature controllers, a Fluke Hydra data logger, and power supplies.

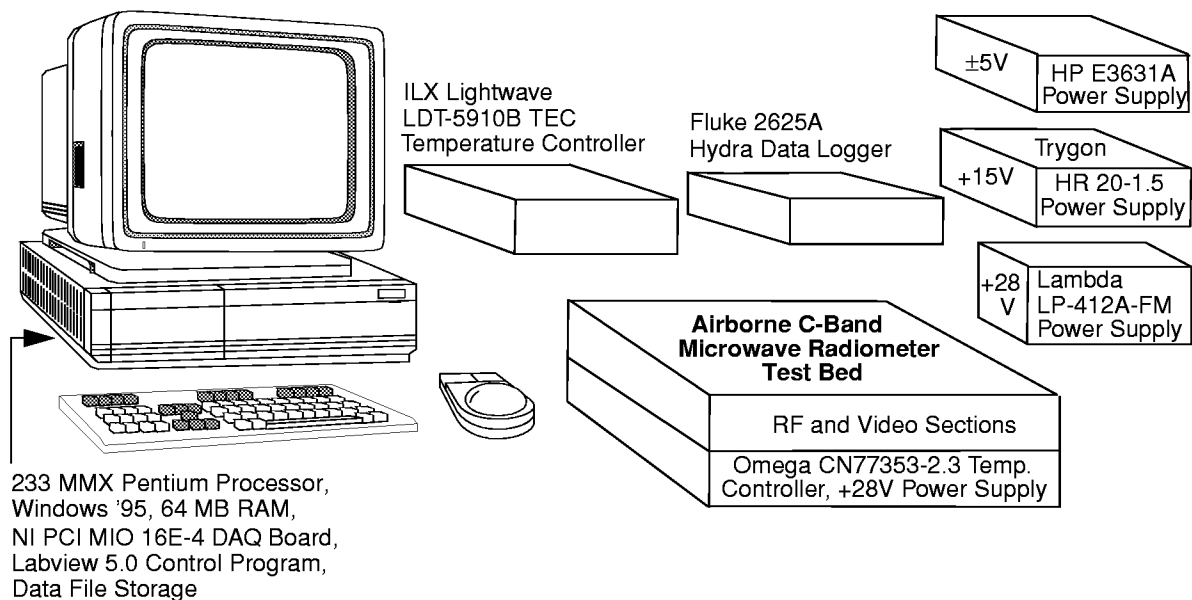


Figure 3. Major components of the experimental radiometer.

Radio Frequency Signal Path

The RF components were housed in the chassis enclosure named "RF and Video Sections." Figure 4 contains a block diagram of the RF signal path through the radiometer; specific RF components are listed in appendix A. A test signal entered the radiometer at the antenna port on the front panel. RF switch 1 switched between an input from the antenna port and an input from an RF termination on the switch at a programmed rate no faster than 5 Hz. This termination was the noise temperature reference; measurements of its noise temperature (372.75 K) were used to monitor and compensate for changes in the system noise temperature in data processing.

RF switch 2 alternately added the output from a calibrated noise diode or a termination through a 30-dB coupler to the input signal; this switch operated at a continuous 10-Hz rate. The coupled noise temperature from the noise diode was 322.67 K. Measurements of the input signal with and without the noise diode allowed for gain and antenna temperature calculations every 0.1 s. The signal then passed through a 28-dB LNA, a 500-MHz filter, and another 28-dB LNA. A square law detector converted the RF signal to a dc signal proportional

to the input noise power. For the expected range of input noise temperatures, 0 to 350 K, this low-barrier, Schottky diode detector operated at a gain of 0.5 mV/ μ W.

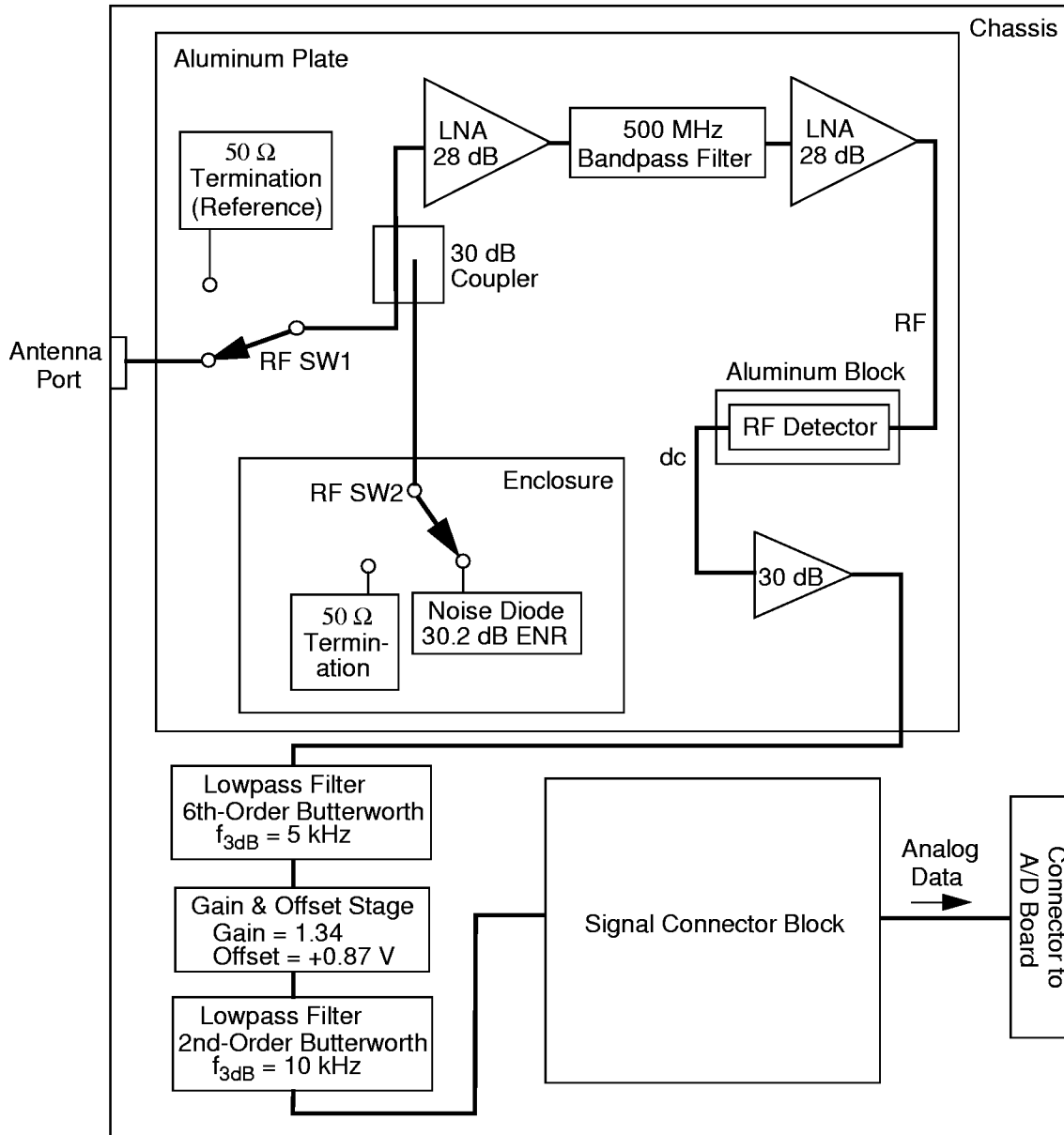


Figure 4. Block diagram of the radiometer RF and dc signal path from antenna port to A/D board connector.

Video Signal Path

As shown in figure 4, the output of the RF detector, a voltage of between 0.1 mV and 1.0 mV, entered a 30-dB-gain amplifier. Schematics for this and other video circuits are shown in appendix B. The amplified signal passed through a 6th-order lowpass Butterworth filter with a cutoff frequency of 5 kHz. This cutoff was determined in accordance with the sampling frequency of 20 kHz. In the gain and offset stage, a small gain (1.34) was applied to the signal,

and a dc offset voltage (+0.87 V) was added to cause the analog data range to fill the range -0.5 V to +0.5 V, for maximum A/D resolution. A final, 2nd-order lowpass Butterworth filter with a cutoff frequency of 10 kHz reduced the effect of any stray clock signals. This frequency was chosen low enough so that the final filter would have a rise time slower than the rise time of the previous, 6th-order Butterworth filter, measured at 0.5 ms. Analog data were routed to the data acquisition board in the PC via the signal connector block and a shielded cable. The data acquisition board contained a programmable input amplifier which amplified the input signal 10 times to fill the range -5.0 V to +5.0 V. The 12-bit conversion of this signal by the A/D allowed for a resolution of 0.244 mV, or 0.19 K prior to averaging, given the system gain of about -1.27 mV/K. Lab power supplies of +5 V, -5 V, +15 V, and +28 V powered the various components.

Temperature Control System

There were two levels of temperature control designed to hold the radiometer physical temperature at 35 C. RF components were mounted on a 9.5 by 11.5 by 1/8 in. aluminum plate, as shown in figure 4, heated by four 2 by 2 in. heating strips placed symmetrically about the underside of the plate. An RTD sensed the plate temperature and sent that information to the Omega proportional-integral temperature controller located in the temperature control chassis enclosure with an SCR voltage amplifier and 28 V power supply. These elements of the temperature control system are detailed in appendix C. The controller output, a voltage between 0 and 10 V dc, was amplified to provide a voltage between 0 and 28 V dc across the parallel connected heater strips. In this way, up to 17 W were provided to the aluminum plate, as needed. Cooling occurred passively, by radiation from the aluminum plate through the metal chassis enclosure. The RF detector was enclosed in an aluminum block in contact with the larger aluminum plate.

The noise diode and RF switch 2 were enclosed in an inner aluminum enclosure mounted on top of the plate inside the main RF and dc section chassis enclosure. A TEC, a thermistor, and an external Lightwave temperature controller regulated the temperature of the small, inner enclosure. Thus, the noise diode and RF switch 2 were doubly temperature controlled. Typically, for a data collection period of 14.5 hr, the laboratory room temperature varied from minimum to maximum by 1.43 C. In response, physical temperatures on the aluminum plate varied about 0.17 C, and inside the noise diode compartment, about 0.04 C. During data recording, physical temperatures measured by three RTD's, one at the noise diode and one at each LNA, were collected by a Fluke Hydra Data Logger and communicated by RS232 bus to the PC for incorporation into the data file every 10 s. The physical temperature of the LNA closest to the reference termination was used to monitor and compensate for changes in the system noise temperature in antenna temperature calculations.

Labview Controls and Digital Recording

By means of an interactive Labview program, the user specified the antenna/reference duty cycle, the A/D sampling rate, the voltage detection range and polarity, and the length of the data recording. The user then started data acquisition and recording. As the program executed, it initiated three TTL clock signals using counter/timers on the DAQ board. These signals were the 250-kHz control clock which set the 6th-order Butterworth filter bandwidth, the RF switch 1 (variable) control clock, and the 20-kHz A/D sampling trigger. A frequency divider (detailed in appendix B) in the chassis enclosure further divided the 20-kHz signal down to a 10-Hz signal to control RF switch 2.

Figure 5 diagrams the relationships among the RF switch timing signals. The RF switch clocks were synchronized with the sampling clock so that ANT and REF portions of the ANT/REF cycle each contained a whole number of 1000-sample groups. In addition, each ANT and REF portion contained a whole number of noise diode cycles, beginning with the noise diode on. Synchronization was accomplished by using the 10-Hz noise diode clock to trigger each cycle of the ANT/REF clock and the beginning of continuous data acquisition at 20 kHz.

Labview also performed calculations on the raw data, displaying gain and antenna temperature results on the monitor and writing data to a file. As analog voltages were sampled at 20 kHz; groups of approximately 1000 samples were averaged every 0.05-s period to obtain the recorded voltages. The first eight data points of each 1000 were ignored while RF switch 2 settled. The recorded data were time of day, voltages, and physical temperatures of the radiometer and room air. Depending on the positions of RF switches 1 and 2, each recorded voltage represented either an antenna or a reference measurement, with or without the addition of the coupled noise diode temperature. A simple antenna temperature calculation was performed as a check in real time; more time-intensive temperature calculations were done in postprocessing.

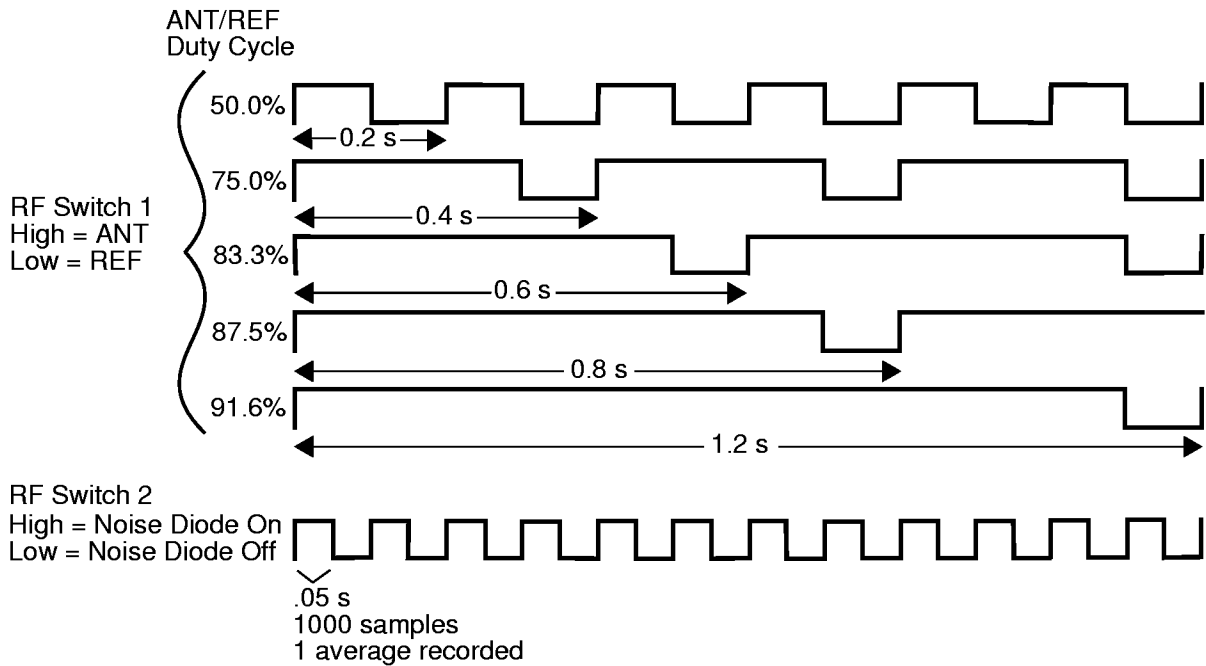


Figure 5. Clock signals for RF switches 1 and 2 during the various ANT/REF duty cycles used to collect data.

Radiometer Characterization: Calibration of System Gain, Noise Diode Temperature, and System Noise Temperature

Calibrations were performed by using two test loads, a Maury model MT7118A Cryogenic Termination at 81.2 K and a Maury model MT7108B Thermal Termination at 372.7 K. The cryogenic termination was cooled by a dewar of liquid nitrogen on one side and heated to a constant 40 C on the other side. An isolation section between the heated mounting plate and the input connector allowed a continuous drop from 40 C to ambient room temperature. The

cryogenic termination's noise temperature was determined to within ± 0.94 K, taking into account the room air temperature, barometric pressure, and mounting-plate temperature. The thermal termination, equipped with a proportional temperature controller, provided a noise temperature also known to within ± 0.94 K. For convenience, the noise temperatures provided by these cold and hot loads will be referred to as T_{COLD} and T_{HOT} . For each calibration, 5 min. of data were recorded and averaged using each reference load. Calibrations were performed on an approximately weekly basis during data gathering. Table 1 contains the average characteristic values for the radiometer, calculated over a three-month period.

Table 1. Radiometer Characteristic Values

Frequency of Detected Input	6.8 GHz
Predetection Bandwidth	500.0 MHz
System Noise Temperature	326.08 K
Physical Temperature/Reference	35.0 C
System Gain	-1.2687 mV/K
Coupled Noise Diode Temperature	322.67 K
A/D Sampling Frequency	20.0 kHz
A/D Resolution	0.2441 mV or 0.1923 K
* Sensitivity with 993-point Averaging	0.1771 K
* Theoretical Balanced Dicke Sensitivity	0.1398 K

* Calculations are for an antenna input of 372.75 K, for 1 hr, using a 50% duty cycle

Radiometer gain was calculated in mV/K as

$$G_{SYS} = \frac{V_{HOT} - V_{COLD}}{T_{HOT} - T_{COLD}} \quad (3)$$

where V_{HOT} was the recorded voltage for the hot termination, V_{COLD} was the recorded voltage for the cold termination, T_{HOT} was the thermal termination temperature, and T_{COLD} was the cryogenic termination temperature.

The noise temperature of energy coupled through the 30-dB coupler from the noise diode was calculated as

$$T_{DIODE} = \frac{(V_{ANT+DIODE+SYS} - V_{ANT+SYS})}{G_{SYS}} \quad (4)$$

where $V_{ANT+DIODE+SYS}$ was the recorded voltage with the noise diode signal added to the input signal, and $V_{ANT+SYS}$ was the recorded voltage with the noise diode signal not added to the input signal.

Figure 6 contains a sketch of the system noise determination procedure. Drawing a line through the two points (V_{COLD}, T_{COLD}) and (V_{HOT}, T_{HOT}) , one obtains a temperature-axis intercept which is the negative of the apparent system noise temperature. If an antenna input of 0 K could be achieved, a voltage equivalent to this system noise temperature would still be recorded at the radiometer output. Because an offset voltage was added to the amplified RF detector output, the noise temperature equivalent to that offset must be subtracted to

determine the actual system noise temperature. The result is the equivalent radiometer noise temperature referred to the antenna port.

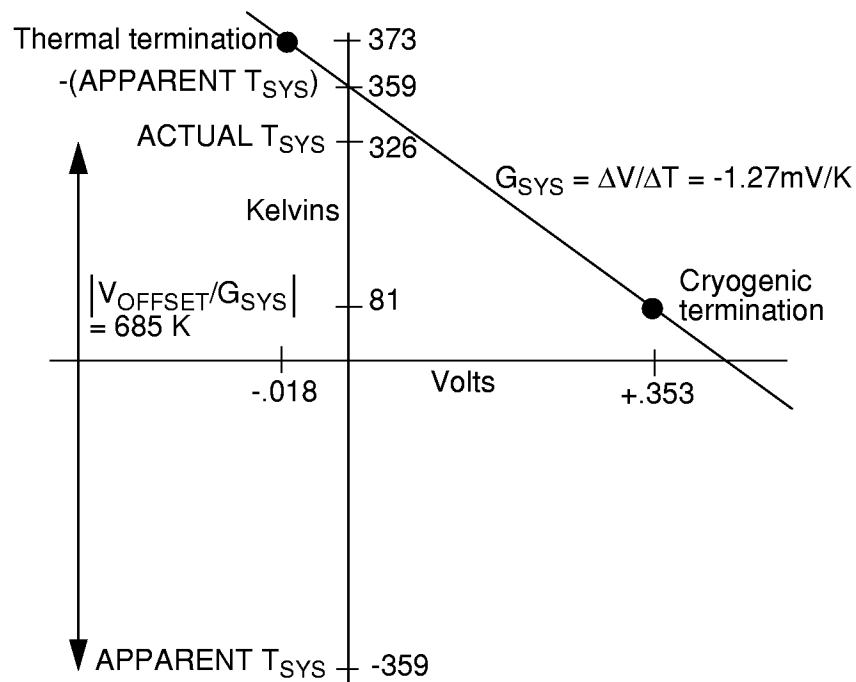


Figure 6. Sketch illustrating a representative system noise temperature determination.

Ulaby, Moore, and Fung [3] give the theoretical sensitivity for a balanced Dicke radiometer as

$$\frac{2(T_{ANT} + T_{SYS})}{\sqrt{B \cdot \tau_s}} \quad (5)$$

where B is the predetection bandwidth and τ_s is the Dicke switching period. Although the experimental radiometer differed from a balanced Dicke radiometer in that half of each antenna and reference cycle were used for noise injection to calculate gain, the theoretical ΔT is given here for comparison to the measured ΔT . For a balanced Dicke radiometer measuring T_{HOT} and using a τ_s of 0.2 s, ΔT would be

$$\frac{(2)(372.75 \text{ K} + 326.08 \text{ K})}{\sqrt{500 \text{ MHz} \cdot 0.2 \text{ s}}} = 0.1398 \text{ K} \quad (6)$$

Experimental measurements of T_{HOT} , using a 50% duty cycle over a period of 0.2 s, with 993-point averaging before recording but with no averaging in postprocessing, yielded an actual variance of 0.03136 K^2 , or a sensitivity of 0.1771 K. In the study, further tests were conducted with the radiometer to determine how much the variance could be further reduced by antenna, reference, and gain averaging.

Comparison of the Effects of Averaging Techniques on Antenna Temperature Variances

Each data set was recorded over a 14.5-hr period; antenna temperature variances were computed for 1-hr intervals, and those results were averaged over the 14 available hours in each data set and over the 3 data sets of each type. Three data sets were recorded at each of the following antenna duty cycles: 50%, 75%, 83.3%, 87.5%, and 91.6%. Antenna temperatures were calculated from the 50% data sets at intervals of 0.2 s, by using antenna averaging; antenna and reference averaging; and antenna, reference, and gain averaging together.

To compare the antenna temperature variances obtainable from higher duty cycles versus those obtainable from a 50% duty cycle, the 50% data sets were next broken into groups of data collected over the same time periods as those used in antenna temperature calculations for the higher duty cycle data sets. For the 75%, 83.3%, 87.5%, and 91.6% duty cycles, respectively, these time intervals were 0.4 s, 0.6 s, 0.8 s, and 1.2 s. Referring to figure 5, one sees that these are the minimum times for which the desired antenna duty cycles existed. The same three 50% data sets, with antenna data averaged over the different intervals, were compared against three data sets of each higher duty cycle, with antenna data averaged over the same intervals. The effect of duty cycle on variance was tested by using antenna averaging; antenna and reference averaging; and antenna, reference, and gain averaging together.

Calculations Common to the Three Averaging Methods

The following sequence of calculations was performed for every antenna temperature calculation. Each time a temperature was desired, G_{SYS} had to be computed first. The required information for this calculation was available at 0.1-s intervals, and gain was calculated either as

$$G_{SYS} = \frac{V_{ANT+DIODE+SYS} - V_{ANT+SYS}}{T_{DIODE}} \quad (7)$$

or as

$$G_{SYS} = \frac{V_{REF+DIODE+SYS} - V_{REF+SYS}}{T_{DIODE}} \quad (8)$$

Antenna temperature was then calculated as

$$T_{ANT} = T_{ANT+SYS} - T_{SYS} \quad (9)$$

To compensate for known changes in the system noise temperature and in the physical reference temperature since the recording started, (9) was rewritten as

$$T_{ANT} = T_{ANT+SYS} - (T_{SYS,INIT} + \Delta T_{SYS}) \quad (10)$$

where

$$T_{ANT+SYS} = \frac{V_{ANT+SYS}}{G_{SYS}} \quad (11)$$

$T_{SYS,INIT}$ was the T_{SYS} computed during calibration described in **Radiometer Characterization**, and

$$\Delta T_{SYS} = \Delta T_{REF+SYS} - \Delta T_{REF} \quad (12)$$

$$= \left(\frac{V_{REF+SYS}}{G_{SYS}} - \frac{V_{REF+SYS,INIT}}{G_{SYS,INIT}} \right) - (T_{REF} - T_{REF,INIT}) \quad (13)$$

T_{REF} was the measured physical reference temperature.

Thus, the Dicke mode was digitally implemented through the subtraction of digitally recorded antenna and reference values. After the antenna temperatures had been calculated for 1 hr of data, the variance of those temperatures was calculated.

Antenna Data Averaging with Variable Duty Cycle

The first averaging technique to be discussed is antenna data averaging. An improved version of this averaging technique was made possible by the variation of antenna duty cycles while recording data. Consider, as an example, the calculation of temperatures from a 75% duty cycle data set. Antenna temperatures were computed from 75% data once every 0.4 s. During the 0.4-s interval, three $V_{ANT+SYS}$ points and one $V_{REF+SYS}$ point were recorded. As a first step in the antenna temperature calculation, the three $V_{ANT+SYS}$ points were averaged. The $V_{REF+SYS}$ point was then averaged with the previous $V_{REF+SYS}$ point and the following $V_{REF+SYS}$ point, so that the reference average represented the same number of integrated points (three) as the antenna average. When this averaging had been done for every 0.4-s interval in the data set, a series of preaveraged antenna and reference points resulted. For comparison to this 75% data set, a 50% data set was broken into 0.4-s groups. In each of the groups the two antenna points were averaged and the two reference points were averaged.

The preaveraged $V_{ANT+SYS}$ and $V_{REF+SYS}$ points were then employed in (11) through (13). For 83.3%, 87.5%, or 91.6% duty cycles, respectively, the numbers of antenna and reference points averaged per interval were 5, 7, and 11. The corresponding 50% data group numbers were 3, 4, and 6. The results are presented both as absolute T_{ANT} variance and as variance normalized to the results for a 50% duty cycle using the same integration times, without reference or gain averaging.

Reference Data Averaging

The second averaging technique is reference averaging. This averaging technique is accomplished entirely by signal processing and may be combined with either of the other two. Here, the reference data are integrated over more points than the antenna data. According to the time for which the reference was stable, an optimal length of rectangular averaging window was found, for which the variance of the computed antenna temperatures was minimal. If the window was longer or shorter than this length, the variance increased again. This optimal length was determined by repeated trial calculations on the same data set. For

the 15 data sets collected in this experiment, the average optimal reference window was 22.7 s. Depending on the duty cycle, a 22.7-s window could include 19 to 57 reference points. A more stable reference would allow the reference data to be averaged over a longer time, providing a greater reduction in variance. As the duty cycle increased and reference points were less frequent, fewer of them could be averaged in the stable window. So, after a point, further increases in duty cycle resulted in more improvement by antenna averaging but in less improvement by reference averaging.

System Gain Averaging

The third averaging technique is system gain averaging. This technique is also accomplished entirely by signal processing and may also be combined with either of the other two. Rather than using a single G_{SYS} for each T_{ANT} calculation, one can average G_{SYS} values going back and forward in time from the corresponding recorded $V_{ANT+SYS}$. For the experimental radiometer, G_{SYS} was stable for 199.9 s. As for the reference window, this length was determined by repeated trial calculations on the same data set. Increasing the rectangular averaging window up to that length of time continuously decreased the variance of the resulting T_{ANT} ; further averaging caused the variance to increase again. After the 1999-point moving average had been applied to the initial series of G_{SYS} values, the averaged series was used in (11) through (13) to compute T_{ANT} , as before.

Results

The results are presented first as absolute T_{ANT} variances, shown numerically in tables 2, 3, and 4 and graphically in figures 7 and 8. Tables 2, 3, and 4 show, in order, the results of antenna averaging; antenna and reference averaging; and antenna, reference, and gain averaging. Each variance is the average result from three data sets at the same duty cycle. In these tables and graphs, “ANT Int. Time” or “ T_{ANT} Integration Time” indicates the interval over which each antenna temperature was calculated. Parts of these intervals were used for the collection of reference, rather than for antenna information. The reported results for reference and gain averaging are the optimum results (least T_{ANT} variances) obtainable for the recorded data sets. Tables 3 and 4 state the number of reference data points averaged to obtain the optimum results by reference averaging. Table 4 states the number of gain points averaged to obtain the optimum result by gain averaging; that number was always 1999 points.

Figure 7 shows the averaged variances for three 50% duty cycle data sets. By recalculating T_{ANT} from the same data integrated over lengthening intervals, one sees a reduction from left to right due to antenna averaging. From top to bottom, one sees the reduction by reference and gain averaging in addition to antenna averaging. By using all three averaging techniques simultaneously, an 88.4% reduction in T_{ANT} variance is effected, from 0.0313 K² to 0.0036 K². This result corresponds to a 65.9% improvement in standard deviation, or sensitivity. Most of the benefit from antenna averaging appears to have been reached by the integration time 1.2 s. For any T_{ANT} integration time, each additional averaging technique further improves the variance. However, the percentage reductions become slightly less for one technique if others have already been applied.

Figure 8 shows the averaged variances for three each of 50%, 75%, 83.3%, 87.5%, and 91.6% duty cycle data sets. Again, the variance decreases from left to right, as antenna integration time increases. However, for each integration time, more points are available from the greater than 50% duty cycle data sets than from the 50% duty cycle data sets, so the

improvement is even more than in figure 7. Using all three averaging techniques simultaneously, a 90.1% reduction in T_{ANT} variance is effected, from 0.0313 K² to 0.0031 K². This reduction corresponds to a 68.5% improvement in standard deviation, or sensitivity. Both curves indicate that antenna data averaging is most beneficial. However, reference and gain averaging are still somewhat beneficial and are very beneficial in the case that it is infeasible to do much antenna averaging.

Table 2. Variance of Calculated T_{ANT} Using Antenna Data Averaging

ANT Duty Cycle (%)	ANT Int. Time (s)	ANT Pts. Aver-aged	REF Pts. Aver-aged	GAIN Pts. Aver-aged	T_{ANT} Variance (K ²)	ANT Duty Cycle (%)	ANT Int. Time (s)	ANT Pts. Aver-aged	REF Pts. Aver-aged	GAIN Pts. Aver-aged	T_{ANT} Variance (K ²)
50.0	0.2	1	1	1	0.0313497						
50.0	0.4	2	2	1	0.0139117	75.0	0.4	3	3	1	0.0108100
50.0	0.6	3	3	1	0.0112053	83.3	0.6	5	5	1	0.0072217
50.0	0.8	4	4	1	0.0074933	87.5	0.8	7	7	1	0.0055817
50.0	1.2	6	6	1	0.0053740	91.6	1.2	11	11	1	0.0042120

Table 3. Variance of Calculated T_{ANT} Using Antenna and Reference Data Averaging

ANT Duty Cycle (%)	ANT Int. Time (s)	ANT Pts. Aver-aged	REF Pts. Aver-aged	GAIN Pts. Aver-aged	T_{ANT} Variance (K ²)	ANT Duty Cycle (%)	ANT Int. Time (s)	ANT Pts. Aver-aged	REF Pts. Aver-aged	GAIN Pts. Aver-aged	T_{ANT} Variance (K ²)
50.0	0.2	1	53	1	0.0209790						
50.0	0.4	2	54	1	0.0100903	75.0	0.4	3	53	1	0.0082057
50.0	0.6	3	51	1	0.0082373	83.3	0.6	5	35	1	0.0058383
50.0	0.8	4	52	1	0.0058810	87.5	0.8	7	33	1	0.0047897
50.0	1.2	6	54	1	0.0044307	91.6	1.2	11	29	1	0.0040017

Table 4. Variance of Calculated T_{ANT} Using Antenna, Reference, and Gain Data Averaging

ANT Duty Cycle (%)	ANT Int. Time (s)	ANT Pts. Aver-aged	REF Pts. Aver-aged	GAIN Pts. Aver-aged	T_{ANT} Variance (K ²)	ANT Duty Cycle (%)	ANT Int. Time (s)	ANT Pts. Aver-aged	REF Pts. Aver-aged	GAIN Pts. Aver-aged	T_{ANT} Variance (K ²)
50.0	0.2	1	53	1999	0.0176360						
50.0	0.4	2	54	1999	0.0093167	75.0	0.4	3	53	1999	0.0067980
50.0	0.6	3	51	1999	0.0065243	83.3	0.6	5	35	1999	0.0047707
50.0	0.8	4	52	1999	0.0050973	87.5	0.8	7	33	1999	0.0038067
50.0	1.2	6	54	1999	0.0036450	91.6	1.2	11	29	1999	0.0031127

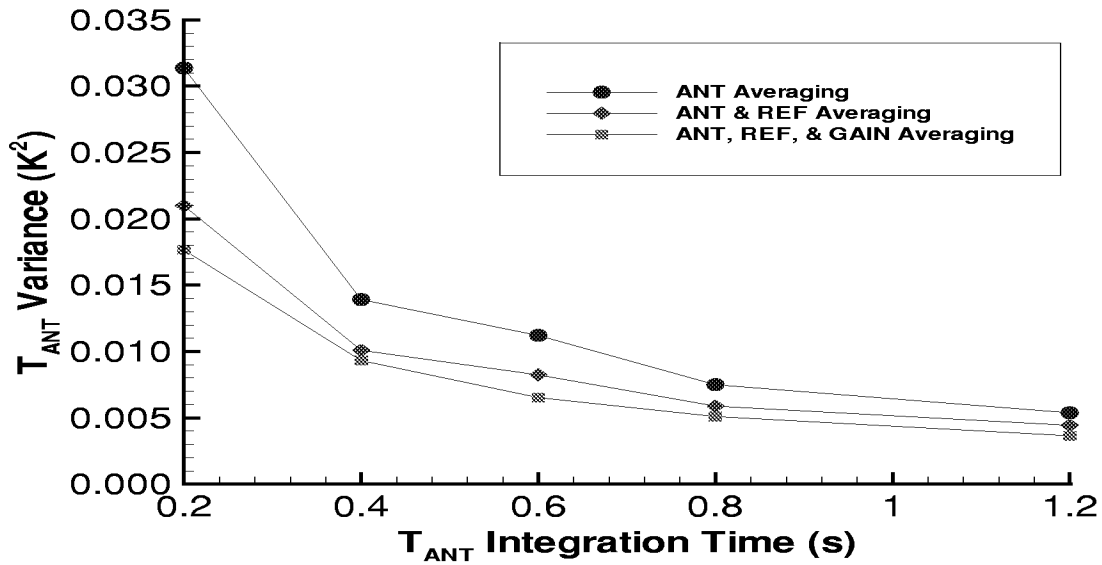


Figure 7. Reduction in variance of T_{ANT} by various averaging techniques for 1 hr of recorded data for which the ANT duty cycle was 50%.

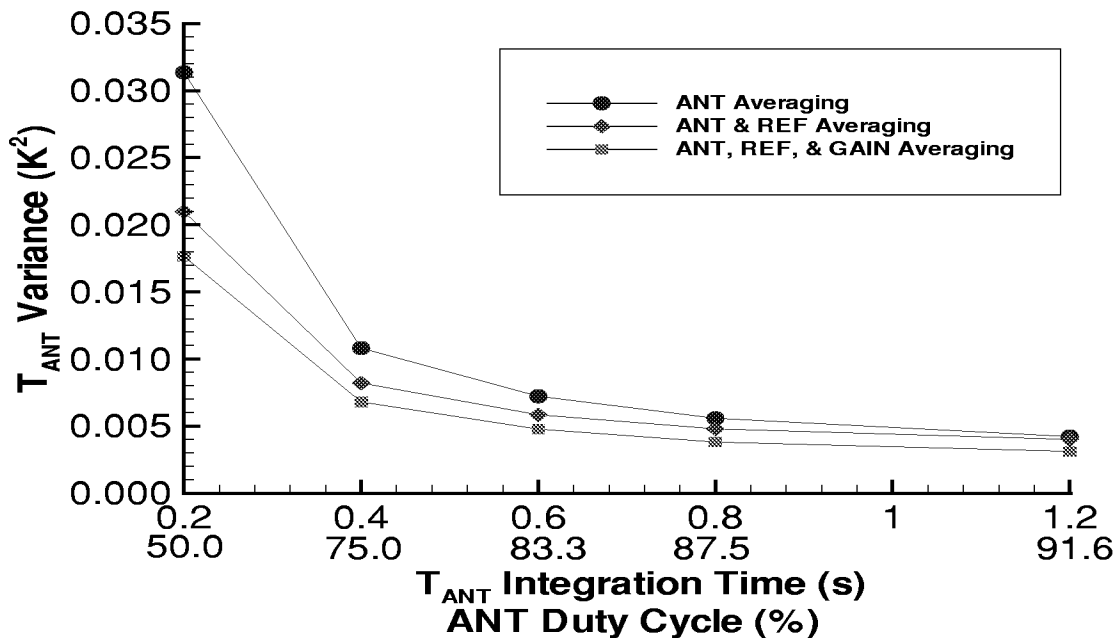


Figure 8. Further reduction in variance of T_{ANT} by increasing the ANT duty cycle before performing other averaging techniques. Compare each point in figure 8 to the similarly marked point above it in figure 7. For example, the variance for the 75% duty cycle is compared against the variance for the 50% duty cycle over the same period, 0.4 s.

Calculation of Improvement for Different Antenna Duty Cycles

To emphasize the reduction in variance by increasing the duty cycle while keeping the same integration time, figure 9 shows the T_{ANT} variances normalized to the variances for the

same integration times, a 50% duty cycle, and no reference or gain averaging. Looking at the normalized results, one sees that for a given integration time, the 83.3% duty cycle affords the most improvement over the 50% duty cycle, a 57.4% reduction in variance. This quantity corresponds to a 34.8% reduction in standard deviation. As the proportion of antenna points increases, the proportion of reference points decreases, and the improvement by reference averaging begins to decrease at duty cycles higher than 83.3%.

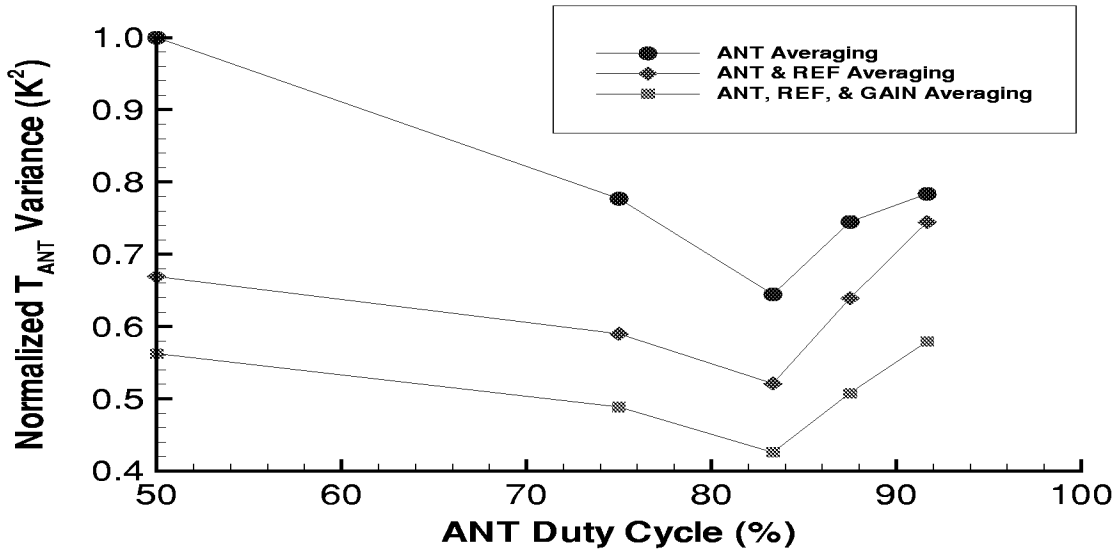


Figure 9. T_{ANT} variance for variable ANT duty cycle, expressed as a fraction of the variance when using the same ANT integration time and 50% duty cycle.

Although each duty cycle variance has been calculated by using a different integration time, this is a valid comparison because the longest integration time, 1.2 s, is within the time period for which noise is entirely white. Figure 10, a graph of the T_{DIFF} Allan variance [5][6], demonstrates the white noise characteristic as a straight line.

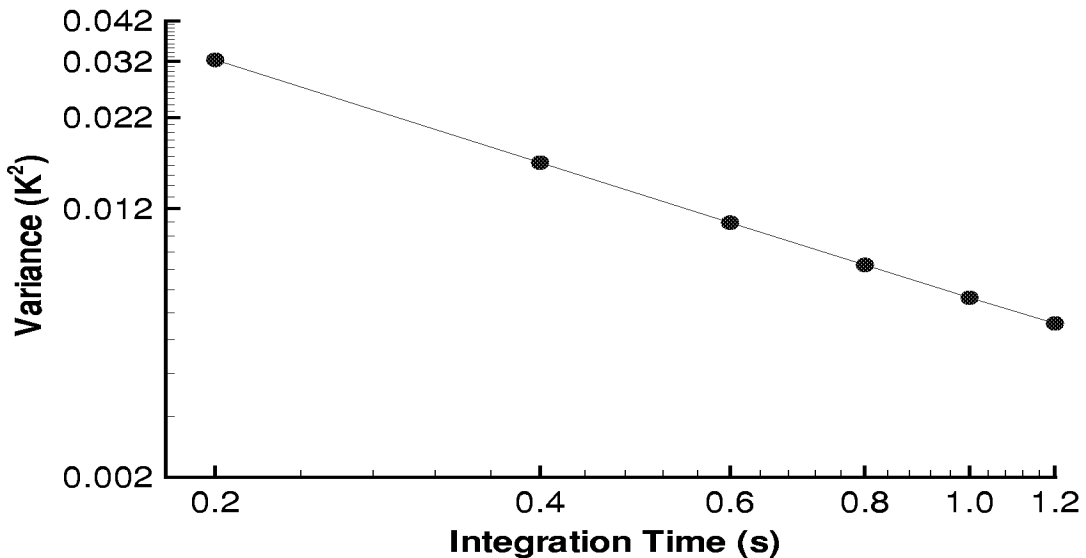


Figure 10. Allan variance of T_{DIFF} for 1 hr of data using a 50% duty cycle. The straight line indicates a white noise characteristic.

The Allan variance technique, detailed in appendix D, calculates the variance of a data set after different numbers of data points have been preaveraged. As long as the log of the variance decreases linearly with the log of the number of points preaveraged, the mean over that number of points has not changed, and the noise present in the data is white noise. The graph in figure 10 is the average of all the 1-hr variances for three 50% duty cycle data sets. T_{DIFF} , the unaveraged, uncompensated difference temperature $T_{ANT+SYS} - T_{REF+SYS}$, is expected to have a variance similar to T_{ANT} and may be calculated more easily. Within this white noise region, variance improvement is dependent only on the proportional increase of integrated antenna points.

Actual Versus Theoretical Reduction in ΔT by Using Asymmetric Chop and Reference Averaging

As stated in the background discussion, the reduction of ΔT white noise, when using asymmetric chop and reference averaging, is predicted by (2). The actual reductions in ΔT , from the results in tables 3 and 4, were compared against the theoretical reductions in cases for which the antenna integration time had been the same but for which the antenna duty cycle or number of averaged reference points had increased. Table 5 compares pairs of data sets for which the antenna duty cycle was the same but for which different numbers of reference points were averaged to calculate T_{ANT} . Table 6 compares pairs of data sets for which both the antenna duty cycle and the number of averaged reference points were different.

Table 5. Reduction in ΔT , Theoretical Versus Actual, for Reference Averaging

ANT Integration Time (s)	ANT Duty Cycle (%)	REF Points Averaged	ANT Duty Cycle (%)	REF Points Averaged	Theoretical Reduction (dB)	Actual Reduction (dB)
0.2	50.0	1	50.0	53	-1.46	-0.87
0.4	75.0	3	75.0	53	-1.39	-0.60
0.6	83.3	5	83.3	35	-1.22	-0.46
0.8	87.5	7	87.5	33	-1.09	-0.33
1.2	91.6	11	91.6	29	-0.81	-0.11

Table 6. Reduction in ΔT , Theoretical Versus Actual, for Asymmetric Chop and Reference Averaging

ANT Integration Time (s)	ANT Duty Cycle (%)	REF Points Averaged	ANT Duty Cycle (%)	REF Points Averaged	Theoretical Reduction (dB)	Actual Reduction (dB)
0.4	50.0	2	75.0	53	-1.64	-1.15
0.6	50.0	3	83.3	35	-1.44	-1.42
0.8	50.0	4	87.5	33	-1.28	-0.97
1.2	50.0	6	91.6	29	-0.95	-0.64

Table 5 shows a rather consistent shortfall in the actual improvements, due to the nonwhite noise present in the reference data being averaged. Table 6, on the other hand, shows much better agreement between the actual and theoretical improvements when reference averaging

was used in conjunction with a greater than 50% antenna duty cycle. For the test radiometer, the ideal reduction in ΔT was achieved by using the 83.3% duty cycle. Recall that figure 9 showed 83.3% to be the most effective duty cycle for the test radiometer at a given integration time.

Conclusions

The experimental Dicke mode radiometer demonstrated several techniques for improving sensitivity. The precision noise-injection gain calibration technique implemented in this radiometer enabled the gain to be continuously measured and corrected with no lost integration time. (Although offset correction was performed in the experiment, the technique is of particular importance in correlation radiometer applications in which no offset correction is required.) The improved gain calibration, together with variable antenna duty cycle and digital averaging, resulted in a reduction in measurement error (improved sensitivity) over the classical 50% Dicke switched radiometer. The enhanced gain calibration concept may improve the performance of large aperture radiometer systems, particularly pushbroom applications, in which longer times may elapse between external calibration events. Also, this concept appears to have application to the ultra-precision requirements for ocean salinity.

In tests with the real radiometer, the greatest sensitivity was achieved by using the highest feasible antenna duty cycle over the longest integration time, for maximum antenna data averaging in conjunction with reference and gain averaging. At a 50% duty cycle, the greatest sensitivity had been obtained at the longest antenna integration time. A more interesting result was that a particular one of the available duty cycles, 83.3%, produced the lowest T_{ANT} variance for any given antenna integration time. The optimum amounts of reference and gain averaging were defined by the stability of those data; in the lab the (average) stable periods were 22.7 s for reference averaging and 199.9 s for gain averaging.

Thus, the optimum sensitivity for the test radiometer depended on two separate processes: the calibration approach allowed the gain and offset corrections to be considered independently and averaged over different time scales. That is, the time averaging for the gain calculation, based on the precision additive noise pulses, was optimized for the gain stability of the system, independent of the offset stability. The time averaging for the reference calculation, based on the Dicke cycle, was optimized for the offset, or reference, stability. Because the optimum duty cycle was dependent on the number of reference data points that could be averaged, the offset stability also determined the amount of antenna averaging.

For a given receiver stability, the performance can be optimized to minimize the overall measurement error. For example, the duration of reference viewing (either internal or external) can be reduced to the minimum time consistent with the specific receiver stability, thus improving the sensitivity. The test results suggest that a radiometer with sufficient reference stability and a sufficiently high sampling rate could operate continuously at a higher than 50% antenna/reference duty cycle, allowing antenna, reference, and gain averaging. Because environmental changes could affect the stabilities in such a way as to change the optimum duty cycle and optimum reference and gain averaging times, the reference and gain stabilities in such an instrument should be recalculated periodically.

Future Work: Stability Analysis of Calculated $T_{REF+SYS}$ and System Gain Using Allan Variances

A further step in developing the digital averaging method will be the real-time assessment of radiometer stability so that the optimum antenna duty cycle and numbers of reference and gain data points can be computed and adjusted for in an automated digital averaging scheme. An automated means for assessing the reference and gain stabilities might include the Allan variance technique. When the reference+system temperature and the system gain are stable over a known period of time, averaging over that period is a valid method of decreasing the variance without affecting the calculated mean, which one wishes to observe over much longer periods.

Figure 11 shows the Allan variance of $T_{REF+SYS}$ for 1 hr worth of data collected at a 50% antenna duty cycle. The initial, sharply descending portion of the curve indicates how long one can expect to be able to average the reference data to advantage in antenna temperature calculations. Most of the improvement by averaging has occurred by 10 s.

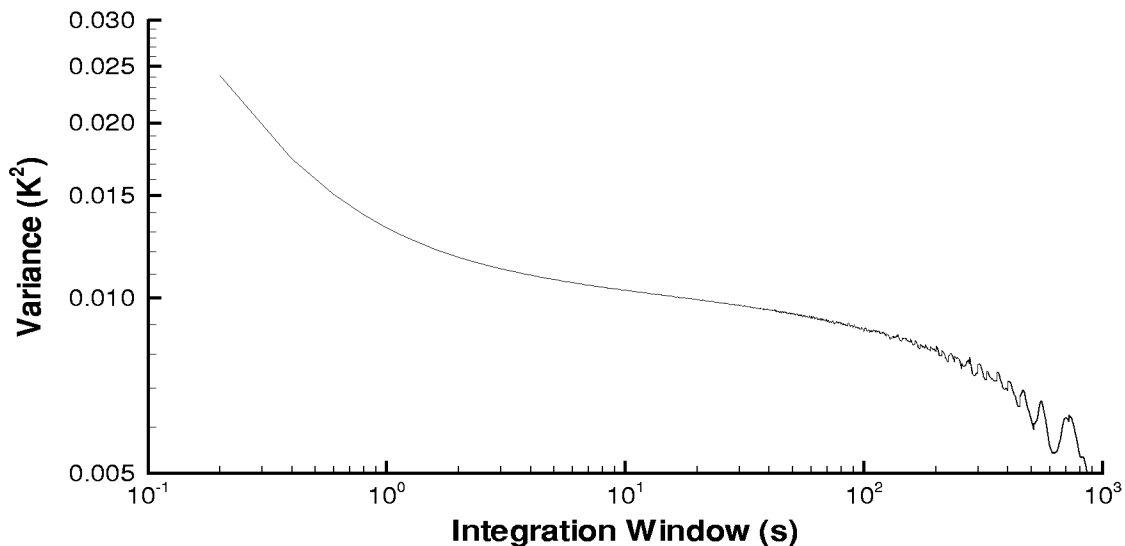


Figure 11. Allan Variance of $T_{REF+SYS}$ for 1 hr of a 50% antenna duty cycle data set, 08/25/99.

Figure 12 shows the Allan variance curve for G_{SYS} , computed for a 1-hr period from the same data set. According to this curve, G_{SYS} is also stable for at least 10 s. It is expected that G_{SYS} would be more stable than $T_{REF+SYS}$ because the gain calculation cancels out T_{SYS} . The result therefore depends only on the noise diode output, which is doubly temperature controlled. The reference calculation, on the other hand, includes T_{SYS} , which is affected by many components in the radiometer which are only singly temperature controlled. It may also be noted that the G_{SYS} Allan variance curve shows a possible reduction of variance by a factor of 33 by averaging, while the $T_{REF+SYS}$ curve shows a possible reduction of variance by a factor of only 2.4.

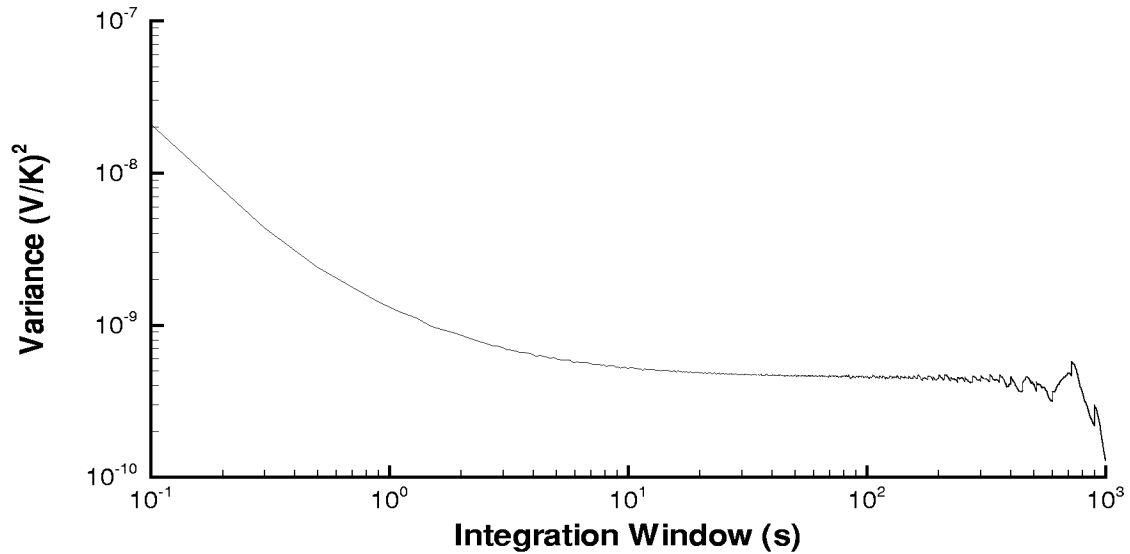


Figure 12. Allan Variance of G_{SYS} for 1 hr of a 50% antenna duty cycle data set, 08/25/99.

Through numerical experiments, it was determined that a benefit could be obtained by averaging reference information for 10.8 s and gain information for 199.9 s for this data set. In more stable data sets, reference information could be averaged for up to 34.8 s, the average being 22.7 s.

Future work will determine the exact relationship between the Allan variance curve and the optimum averaging periods. In addition, it will be necessary to determine how often the averaging algorithms should be updated and how much past information is needed to perform each update.

Appendix A RF Component List

<u>Part Name</u>	<u>Quantity</u>	<u>Manufacturer</u>	<u>Part Number</u>
SPDT RF Switch	2	Mid-Atlantic RF Systems, Inc.	SPDC 965
30-dB-ENR Noise Diode	1	Noise Comm	NC 3103C
30-dB Directional Coupler	1	Merrimac	CSM-30M-6G
28-dB LNA	2	JCA Technology, Inc.	JCA 67-350
500-MHz Bandpass Filter	1	Daden-Anthony Associates, Inc.	6800-550-3SS
RF Detector	1	Hewlett-Packard	HP 8472B

Appendix B Electronic Board Schematics

These video circuits in figures B1 through B4 were fabricated on small circuit boards and placed inside the chassis enclosure with the RF section of the radiometer.

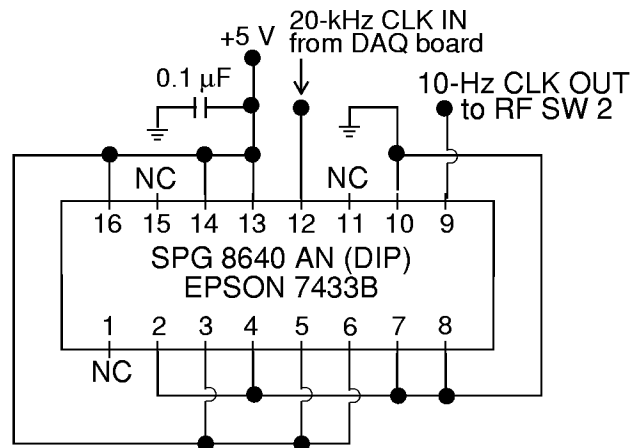


Figure B1. Frequency divider.

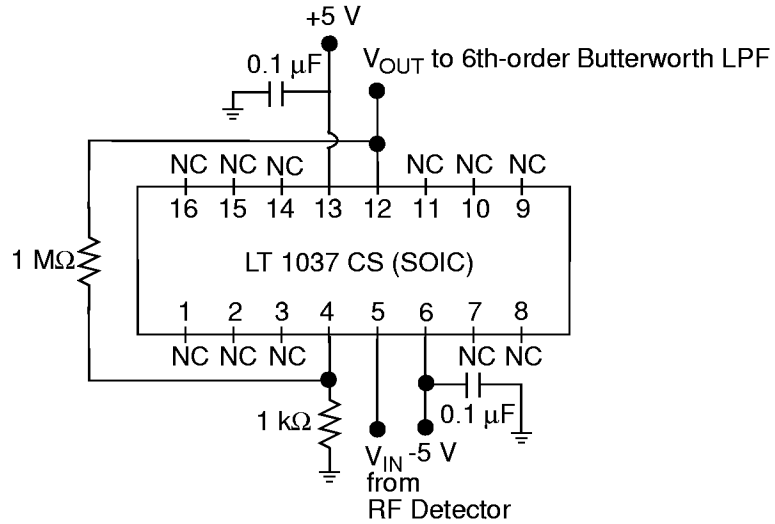


Figure B2. Voltage amplifier, 30-dB-gain.

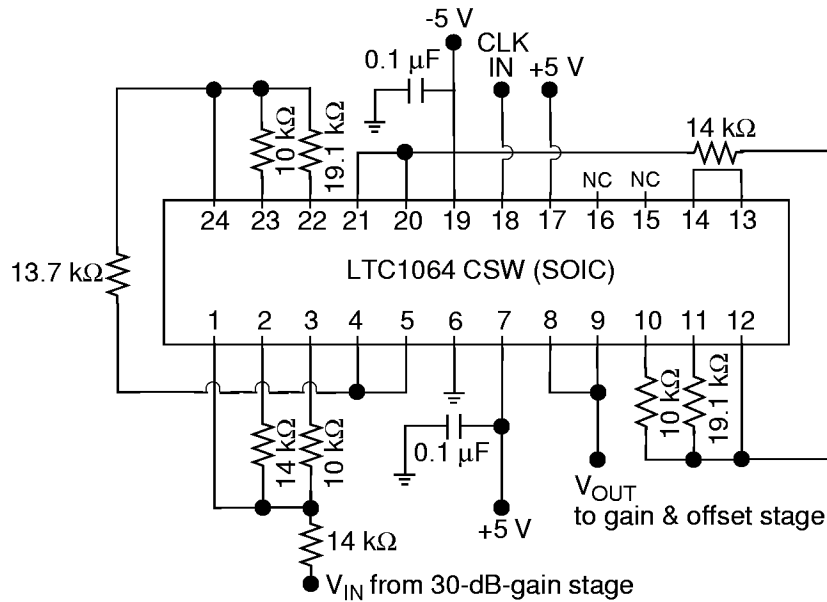


Figure B3. Sixth-order Butterworth lowpass, switched capacitor filter. In this mode, the programmable CLK input (250 kHz) from the DAQ board was divided by 50 to determine the 3-dB bandwidth.

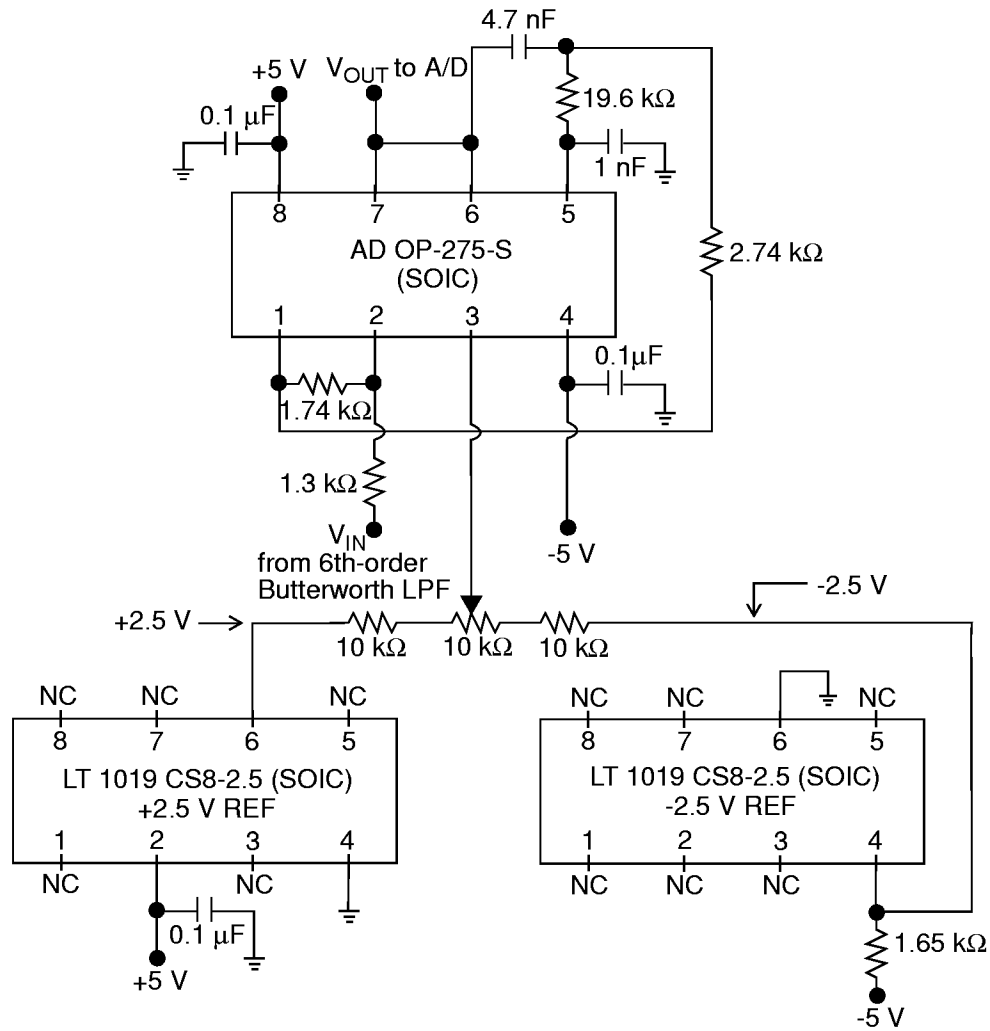


Figure B4. Voltage gain and offset adjustment /2nd-order Butterworth lowpass filter. The dual op amp AD OP-275-S performed both functions.

Appendix C Temperature Control System Schematic

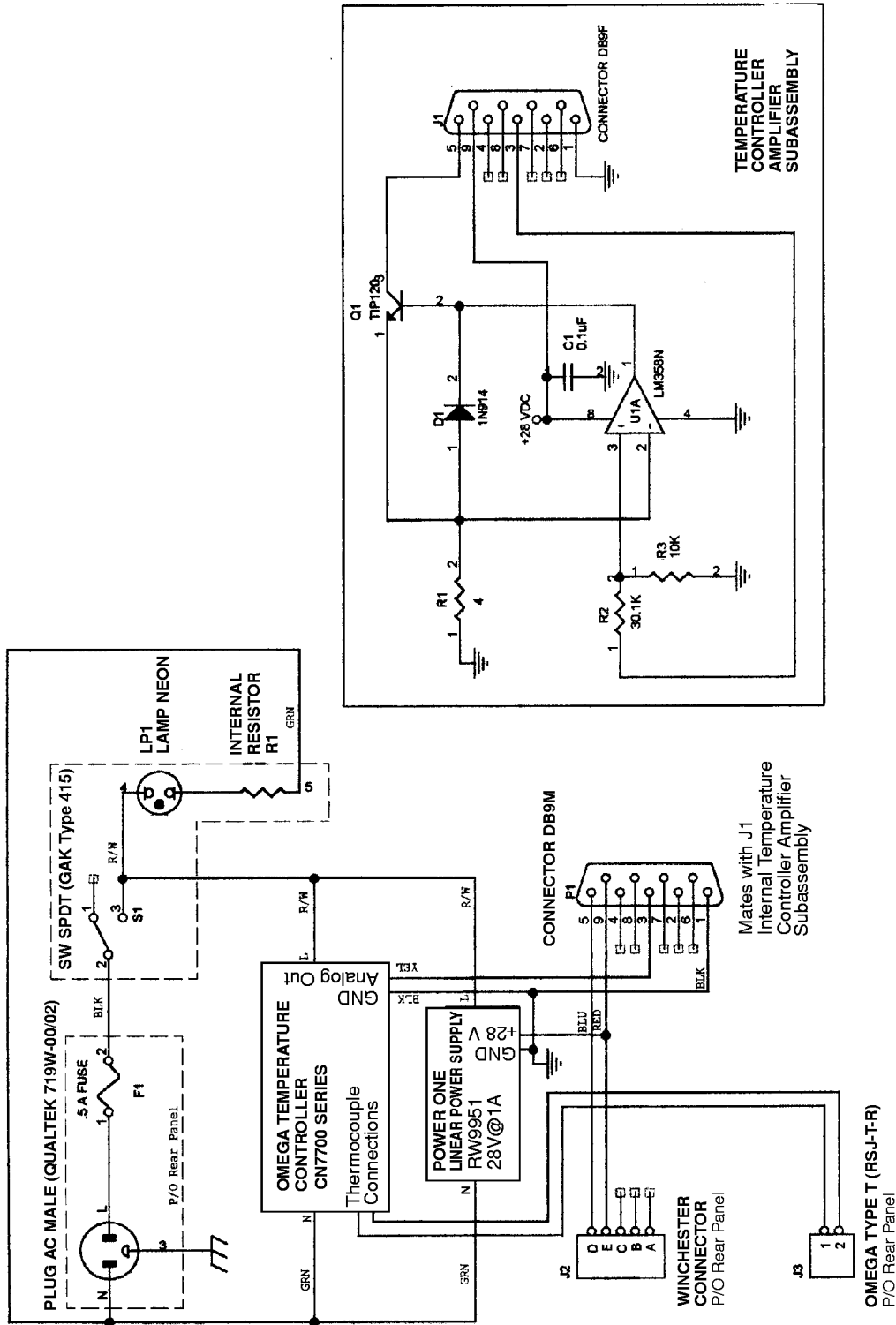


Figure C1. Temperature control system components located in the temperature control chassis enclosure.

Appendix D

Allan Variance

The Allan variance is a statistical method for determining the variance of a random process in terms of the number of samples that have been averaged prior to computing the variance. The calculation is done as follows:

The process is sampled at regular intervals to provide N samples $x(n\Delta t)$. The series of samples is broken into M subgroups of samples, each subgroup having length N/M . Each subgroup is averaged to provide the averaged series having terms

$$y_m = \frac{M}{N} \sum_{n = m(N/M)}^{(m+1)(N/M) - 1} x(n\Delta t) \quad (D1)$$

The sample variance of y is computed as

$$\sigma^2(y) = \frac{1}{M-1} \sum_{m=0}^{M-1} \left[y_m - \frac{1}{M} \sum_{m=0}^{M-1} y_m \right]^2 \quad (D2)$$

and is known as the Allan variance of $x(n\Delta t)$. $(N/M)\Delta t$ defines the time interval τ for which the Allan variance has been computed. The Allan variance is recomputed for increasing values of τ , and typically the result is plotted as $\log(\sigma^2)$ versus $\log(\tau)$. To save computation time and because the variance of white noise is halved as τ is doubled, τ is often increased as powers of 2. As τ increases, the number of subgroups M decreases, and the Allan variance becomes less meaningful.

Lawrence, Scherner, and Grady [5] described the uses and implementation of the method as it applies to radiometer stability. Stanley [6] wrote an efficient algorithm for the calculation of a “two-point” Allan variance and tested that method to identify noise as white, $1/f$, or random walk.

References

1. Hollinger, J.; Lo, R.; and Poe, G.; Naval Research Laboratory; Savage, R. and Pierce, J.; Hughes Aircraft Company: Special Sensor Microwave/Imager User's Guide, Naval Research Laboratory, Washington, D.C., September 14, 1987, pp. 1-37.
2. Njoku, E. G.; Rahmat-Samii, Y.; Sercel, J.; Wilson, W. J.; and Moghaddam, M.: Evaluation of an Inflatable Antenna Concept for Microwave Sensing of Soil Moisture and Ocean Salinity. *IEEE Transactions on Geoscience and Remote Sensing*, vol. 37, no. 1, January 1999, p. 63.
3. Ulaby, Fawwaz T.; Moore, Richard K.; and Fung, Adrian K.: *Microwave Remote Sensing, Active and Passive, Volume 1: Microwave Remote Sensing Fundamentals and Radiometry*. Addison-Wesley Publishing Company, Inc., Reading, Massachusetts, 1981, pp. 369-374.
4. Bremer, James C.: Improvement of Scanning Radiometer Performance by Digital Reference Averaging. *IEEE Transactions on Instrumentation and Measurements*, vol. 1M-28, no. 1, March 1979, pp. 46-54.

5. Lawrence, Roland W.; Scherner, Michael J.; and Grady, Benjamin M.: Measurement of Calibration Stability of Radiometer Systems. *1993 SPIE International Symposium on Optical Engineering and Photonics in Aerospace and Remote Sensing*, April 12-16, 1993.

6. Stanley, William D.: Investigation of Allan Variance for Determining Noise Spectral Forms With Application to Microwave Radiometry. NASA CR 194985, November 1994.

Related Reading

Hersman, Michael S. and Poe, Gene A.: Sensitivity of the Total Power Radiometer with Periodic Absolute Calibration. *IEEE Transactions on Microwave Theory and Techniques*, vol. MTT-29, no. 1, January 1981, pp. 32-40.

REPORT DOCUMENTATION PAGE

*Form Approved
OMB No. 0704-0188*

Public reporting burden for this collection of information is estimated to average 1 hour per response, including the time for reviewing instructions, searching existing data sources, gathering and maintaining the data needed, and completing and reviewing the collection of information. Send comments regarding this burden estimate or any other aspect of this collection of information, including suggestions for reducing this burden, to Washington Headquarters Services, Directorate for Information Operations and Reports, 1215 Jefferson Davis Highway, Suite 1204, Arlington, VA 22202-4302, and to the Office of Management and Budget, Paperwork Reduction Project (0704-0188), Washington, DC 20503.

1. AGENCY USE ONLY (Leave blank)		2. REPORT DATE May 2000	3. REPORT TYPE AND DATES COVERED Technical Memorandum	
4. TITLE AND SUBTITLE Three Averaging Techniques for Reduction of Antenna Temperature Variance Measured by a Dicke Mode, C-Band Radiometer			5. FUNDING NUMBERS RTA 258-70-21-06	
6. AUTHOR(S) Anne I. Mackenzie and Roland W. Lawrence				
7. PERFORMING ORGANIZATION NAME(S) AND ADDRESS(ES) NASA Langley Research Center Hampton, VA 23681-2199			8. PERFORMING ORGANIZATION REPORT NUMBER L-17987	
9. SPONSORING/MONITORING AGENCY NAME(S) AND ADDRESS(ES) National Aeronautics and Space Administration Washington, DC 20546-0001			10. SPONSORING/MONITORING AGENCY REPORT NUMBER NASA/TM-2000-210283	
11. SUPPLEMENTARY NOTES				
12a. DISTRIBUTION/AVAILABILITY STATEMENT Unclassified—Unlimited Subject Category 35 Distribution: Standard Availability: NASA CASI (301) 621-0390			12b. DISTRIBUTION CODE	
13. ABSTRACT (Maximum 200 words) As new radiometer technologies provide the possibility of greatly improved spatial resolution, their performance must also be evaluated in terms of expected sensitivity and absolute accuracy. As aperture size increases, the sensitivity of a Dicke mode radiometer can be maintained or improved by application of any or all of three digital averaging techniques: antenna data averaging with a greater than 50% antenna duty cycle, reference data averaging, and gain averaging. An experimental, noise-injection, benchtop radiometer at C-band showed a 68.5% reduction in ΔT after all three averaging methods had been applied simultaneously. For any one antenna integration time, the optimum 34.8% reduction in ΔT was realized by using an 83.3% antenna/reference duty cycle.				
14. SUBJECT TERMS Microwave radiometer; Remote sensing; Dicke mode; Noise injection; Digital averaging; Antenna averaging; Reference averaging; Gain averaging; Increased sensitivity; Stability; Allan variance			15. NUMBER OF PAGES 34	
			16. PRICE CODE AO3	
17. SECURITY CLASSIFICATION OF REPORT Unclassified	18. SECURITY CLASSIFICATION OF THIS PAGE Unclassified	19. SECURITY CLASSIFICATION OF ABSTRACT Unclassified	20. LIMITATION OF ABSTRACT UL	